

The Rayleigh-Haring-Tayfun distribution of wave heights in deep water

S. Mendes^{a,b}, A. Scotti^b

Non-peer-reviewed preprint submitted to Applied Ocean Research

^a*Group of Applied Physics and Institute for Environmental Sciences, University of Geneva, Blvd. Carl-Vogt 66, Geneva, Switzerland*

^b*Department of Marine Sciences, University of North Carolina at Chapel Hill, Chapel Hill, NC, 27599 USA*

Abstract

Regarding wave statistics, nearly every known exceeding probability distribution applied to rogue waves has shown disagreement with its peers. More often than not, models and experiments have shown a fair agreement with the Rayleigh distribution whereas others show that the latter underpredicts extreme heights by almost one order of magnitude. Virtually all previous results seem to be microcosms, special cases of the underlying essence of this phenomenon. The present work focuses on the apparent contradiction among the majority of previous works. Based on the issue of strong uneven distribution of rogue waves found in [Stansell \(2004\)](#), a new exceeding probability distribution for rogue waves and the analysis of their uneven occurrence is conceived. The proposed distribution is a geometrical composition of the most popular models for wave records ([Longuet-Higgins, 1952](#); [Haring et al., 1976](#); [Tayfun, 1980](#)) with additional algebraic structures. The suggested distribution also obeys empirical physical bounds obtained from the analysis of nearly 350,000 waves from storms recorded in North sea and supports the qualitative likelihood of appearance interpretation based on the symbiosis among three sea state parameters.

Keywords: Rogue Wave, Exceeding Probability Distribution, Composition Law, Water Wave, Storms, Nonlinearity, Physical Bounds

1. Introduction

The seminal work of [Longuet-Higgins \(1952\)](#) introduced a Rayleigh distribution (normal) of wave heights for a narrow-banded sea, henceforth abbreviated as RD. The observation of the so-called Draupner wave in the mid '90s brought a renewed interest on the subject of rogue waves ([Haver and Andersen, 2000](#); [Haver, 2004](#)), whose unusually large amplitude and steepness seem to appear out of nowhere ([Akhmediev et al., 2009b](#)). Naturally, one of the most important considerations for marine safety of offshore operations and ship traffic is the recurrence interval of extreme waves in a particular sea state, also known as the return period, i.e. the required number of waves for each observed rogue wave. The accurate forecast of rogue waves return period is paramount because these waves cause a lot of damage to the industry ([Faukner, 2002](#); [Cruz and Krausmann, 2008](#)). Given the numerous examples of the destructive power of rogues, marine safety is one of the main concerns and purposes of this study. As such, the drive to obtain cutting-edge knowledge about oceanographic, mathematical and meteorological conditions for ship and offshore standards has received increased focus and importance over the last decade. Therefore, the complete understanding of all possible physical processes of generation, modeling of the exceeding probability as well as the creation of an accurate warning system for diametrical sea states are essential for the design of both marine installations and ships.

Due to both randomness in the forcing mechanism and the nonlinear dynamics underlying the evolution of the wave field, a description of the sea state is necessarily statistical in nature. The statistical approach leading to the RD describes the sea surface as a superposition of wavelets with different frequencies and directional spreading. The simplest configuration of this group of waves is the assumption of a uniform distribution of wave phases. Although

Email addresses: saulo.dasilvamendes@unige.ch (S. Mendes), ascotti@unc.edu (A. Scotti)

these approximate formulations have shown remarkable success in describing general ocean wave statistics and kinematics, some issues arise and is our interest to understand the deviation from these models that lead to the formation of rogue waves in the upper tail of the distribution. For instance, based on RD, Øistein (2002) predicts that the famous Draupner wave crest would appear only within a group of a million waves, almost two orders of magnitude higher than the observed number of waves during the Draupner storm (Trulsen and Dysthe, 1997; Haver and Andersen, 2000; Haver, 2004).

Noticing the inaccuracy of the RD model prediction, strongly nonlinear mechanisms have been proposed to fill the gaps in the standard model (Kharif and Pelinovsky, 2003; Dysthe et al., 2008; Onorato et al., 2013). Among these nonlinear models, the so-called Nonlinear Schrödinger equations (NLSE) stand out as the most popular and studied. They have been widely used to model rogue waves for the last three decades (Peregrine, 1983; Janssen, 2003), particularly in the context of unidimensional water wave fields (Akhmediev and Korneev, 1986; Akhmediev et al., 2009a). NLS-type equations can be readily derived from the Euler equations if one assumes weak nonlinearity (small steepness) and narrow-banded spectrum. A remarkable example of such derivation is the Zakharov equation that assumes weak nonlinearity but deals with generalized bandwidth (Zakharov, 1968). Several other types of NLSE have been studied, including the Dysthe and Davey-Stewartson equations (Davey and Stewartson, 1974; Dysthe, 1979). Nevertheless, the mathematical physics of the NLSE and related subjects have not yet been applied to the task of prediction and warning system, but of rogue wave formation alone. However, this nonlinear mechanism has shown limited success in explaining the formation of rogue waves. For instance, Fedele et al. (2016) explains that typical oceanic wind seas features multidirectional wave fields which spreads the energy directionally thus diminishing the effect of both modulational instability and/or nonlinear focusing, which are the established as the main mechanisms of rogue wave formation. Moreover, the role of these instabilities in the formation of rogue waves appear of lesser importance in finite depths. Secondly, theoretical analysis of third-order quasi-resonant interactions in Janssen (2003) play a negligible role in rogue wave formation in realistic sea states (Fedele, 2015). Besides, these approximations seem to lose importance when the steepness becomes large and their amplification by means of breathers are greatly diminished. Nonetheless, these seemingly contradictory views could be unified (Dematteis et al., 2018, 2019).

On the other hand (in a non-exhaustive bibliography), more down-to-earth models have been proposed in the meantime, with not less than a few dozen distributions have been proposed (Jahns and Wheeler, 1973; Haring et al., 1976; Forristall, 1978; Tayfun, 1980, 1983; Ochi, 1986; Langley, 1987; Winterstein, 1988; Tayfun and Lo, 1989; Tayfun, 1990; Kriebel and Dawson, 1991; Ochi and Ahn, 1994; Winterstein et al., 1994; Cieslikiewicz, 1998; Kobayashi et al., 1998; Srokosz, 1998; Forristall, 2000; Song et al., 2002; Prevosto and Bouffandeau, 2002; Krogstad and Barstow, 2004; Socquet-Juglard et al., 2005; Tayfun and Fedele, 2007). Most of these distributions include Stokes second-order terms and the probability distribution is expressed in terms of the significant steepness and wave heights and may include a depth parameter for shallow water waves (see Tayfun and Alkhalidi (2020) for a review on their methodological differences). Additional methods have been applied such as Gram-Charlier expansions (Longuet-Higgins, 1963; Al-Humoud et al., 2002; Mori and Yasuda, 2002) which highlights the importance of the skewness and excess kurtosis of the surface elevation. Although an approach based on the Gram-Charlier covers water waves of any bandwidth, it suffers from being computationally burdensome. In addition, this approach produces undesirable negative probabilities and bounds for maximum and minimum surface elevations that are not compatible with the physics of the system (Forristall, 2000).

Despite the joint effort of several leading academic and private groups and in creating research projects to obtain further understanding of this phenomenon, no consensus regarding the exceeding probability for rogue wave heights or crests nor its generation mechanism has been reached (Bitner-Gregersen and Gramstad, 2015; Karmpadakis et al., 2020). Furthermore, the lack of consensus inevitably leads to a hold on any intention to update offshore standards by classification societies. Historically, the Agulhas current off of the southeast coast of South Africa has been the first site where rogue waves could be easily identified (Mallory, 1974), nevertheless, specific sea state parameters as well as other generation mechanisms implemented over that region did not reach success in predicting rogue waves (Bitner-Gregersen and Gramstad, 2015). Likewise, the MaxWave project (Savina et al., 2003) proposed the implementation of indices that coupled significant wave height and wave steepness as well as directional spreading as a warning system for rogue waves in the weather forecasting. The suggested major index was mostly dependent on the significant steepness (undefined in Savina et al. (2003)) and the significant wave height $H_{1/3}$, i.e. the mean wave height among the 1/3 highest waves recorded in the time series. The two indices were implemented by Meteo France and the occurrence of rogue waves was found to be weakly correlated with them. Numerous authors have attempted

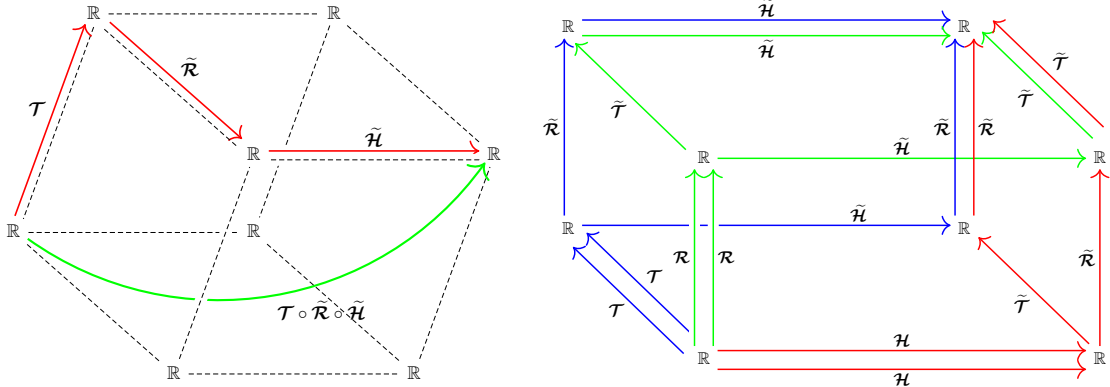


Figure 1: (Left) Graphic representation of the aimed composition rule as a three-dimensional $f \circ g$ and (Right) Possible compositions spanning all paths over the cube edges.

to link spectral parameters and the occurrence of rogue waves with similar dire results, making the current state of warning system not satisfactory (Bitner-Gregersen and Gramstad, 2015). Therefore, In this work we attempt to devise an exceeding probability that explains the uneven spread of rogues among several storms as described by Stansell (2004) and at the same time obey the physical limits obtained from the data (Mendes et al., 2021), whose dataset did not include information on the directionality for the analysis, which can indeed affect the results obtained thereof. The reader is referred to the most important references regarding experimental (Onorato et al., 2009; Waseda et al., 2009; Toffoli et al., 2017) and numerical (Toffoli et al., 2008, 2009) analysis of the role of directionality and sea state parameters affecting rogue wave statistics.

2. Rayleigh-Haring-Tayfun Model

The analysis in Mendes et al. (2021), which is also indispensable to follow the notation in this study, has described Stansell's data in detail and highlighted the unevenness of the observed return period into further minutiae. We advocate for the formulation of a distribution built through a geometrical composition that approaches the RD in the appropriate limit. In view of the shortcomings of the distributions highlighted in chapter Mendes et al. (2021), we will use a different strategy: we start with a narrow-band approximation of the geometrical composition followed by the inclusion of nonlinear effects as a final step. Individually, the recovery of RD is achievable in limiting conditions except for the Forristall (1978, 2000) models. Such constraint will be key to decide the final version of the sought distribution. Regardless of the choice for the composition, equation (1) must recover the normal distribution. Let the composition function be of the type (see figure 1):

$$\mathbb{P}_\alpha = (\mathcal{J}_i \circ \mathcal{J}_j) \circ \mathcal{J}_k \equiv \mathcal{J}_{ijk} \quad ; \quad \lim_{\varepsilon \rightarrow 0} \mathcal{T}(H > \alpha H_{1/3}) = \mathcal{R}_\alpha \quad ; \quad \lim_{\varepsilon \rightarrow 0} \mathcal{H}(H > \alpha H_{1/3}) = \mathcal{R}_\alpha \quad . \quad (1)$$

With that in mind, we write a general expression for the distribution structure \mathcal{J}_{ijk} ,

$$\mathcal{J}_{ijk} = \exp \left[- \frac{A}{\varepsilon^{2+\delta}} \left(\sqrt{1 + \alpha \mathcal{H}_0 \varepsilon^\theta} - 1 \right)^{2+\tilde{\delta}} \right], \quad \mathcal{H}_0 = - \frac{\ln \mathcal{H}_\alpha}{2\alpha^2} = \left(1 - 1.24 \varepsilon \alpha + 1.09 \varepsilon^2 \alpha^2 \right). \quad (2)$$

where \mathcal{H}_0 is the Haring root function. Then, we must find unique values for A , θ and $\tilde{\delta}$ for a given δ that fulfills the Rayleigh-Haring-Tayfun limit:

$$\lim_{\substack{\varepsilon \rightarrow 0 \\ \delta \rightarrow 0}} \frac{A}{\varepsilon^{2+\delta}} \left(\sqrt{1 + \alpha \mathcal{H}_0 \varepsilon^\theta} - 1 \right)^{2+\tilde{\delta}} = 2\alpha^2 \quad . \quad \therefore \quad \frac{A \cdot \theta^2 \alpha^2}{4(2 + \delta - \theta)} \left(\frac{2 + \tilde{\delta}}{2 + \delta} \right) \lim_{\varepsilon \rightarrow 0} \frac{\varepsilon^{2\theta-2-\delta}}{(1 + \alpha \varepsilon^\theta)^{-3/2}} = 2\alpha^2 \quad . \quad (3)$$

Accordingly, we find $\theta = 1 + \delta/2$ the solution $(A, \delta, \tilde{\delta}, \theta)$ must be equal to $(8, 0, 0, 1)$. In addition, Mendes et al. (2021) introduced physical bounds for the variables α , ε and ε , so that the following criteria should be fulfilled by established

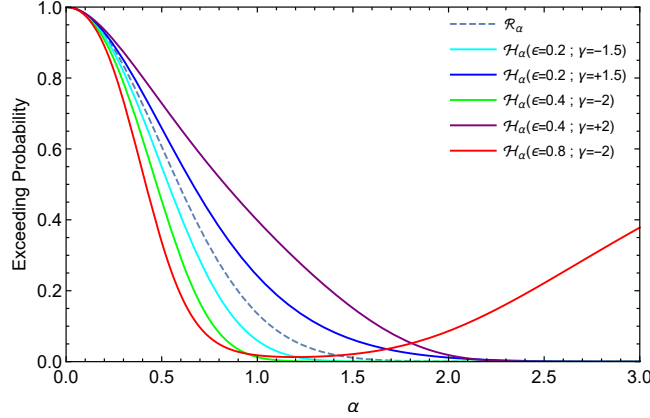


Figure 2: Adjustment to [Haring et al. \(1976\)](#) by a factor γ as in eq. (8).

and forthcoming probability distributions:

$$\mathbb{P}_\alpha(\alpha > \alpha_\infty) \longrightarrow 0 \quad ; \quad \mathbb{P}_\alpha(\varepsilon > \varepsilon_\infty) \longrightarrow 0 \quad ; \quad \mathbb{P}_\alpha(\varepsilon\alpha > \|\varepsilon\alpha\|_\infty) \longrightarrow 0 \quad . \quad (4)$$

Following eq. (3), it is plain to find an expression for such an operation (see figure 1):

$$\tilde{f} := \left| \sqrt{-\frac{1}{2} \ln f} \right| \quad \therefore \quad \mathcal{R}(\tilde{\mathcal{R}}(\alpha)) = \mathcal{R}(\alpha) := e^{-2\alpha^2} \quad . \quad (5)$$

Hence, the composition law of RD with another function $\mathcal{J}(\alpha)$ would produce,

$$(\mathcal{J} \circ \tilde{\mathcal{R}})_\alpha \equiv \mathcal{J}(\tilde{\mathcal{R}}(\alpha)) = \mathcal{J}(\alpha) \quad \therefore \quad \lim_{\substack{\varepsilon \rightarrow 0 \\ \varepsilon \rightarrow 0}} \mathcal{T}(\alpha) \circ \tilde{\mathcal{H}}(\alpha) = \lim_{\substack{\varepsilon \rightarrow 0 \\ \varepsilon \rightarrow 0}} \mathcal{H}(\alpha) \circ \tilde{\mathcal{T}}(\alpha) = \mathcal{R}(\alpha) \quad . \quad (6)$$

Discarding cumbersome looking combinations and taking into account the constraint in eq. (3) as well as changing the steepness from ε to ε , the best version for eq. (2) is:

$$\mathbb{P}_\alpha = \mathcal{T}(\tilde{\mathcal{R}}(\tilde{\mathcal{H}}(\alpha))) = \exp \left\{ -\frac{8}{\varepsilon^2} \left[\sqrt{1 + \varepsilon\alpha\mathcal{H}_0^{1/2}} - 1 \right]^2 \right\} \quad , \quad (7)$$

which we call the Rayleigh-Haring-Tayfun (RHT) model. It recovers [Tayfun \(1980\)](#) when $\varepsilon \rightarrow 0$, [Haring et al. \(1976\)](#) when $\varepsilon \rightarrow 0$ and [Longuet-Higgins \(1952\)](#) when both variables vanish, as intended. Since the negligible variability for [Haring et al. \(1976\)](#) and [Tayfun \(1980\)](#) in response to sea states is well-known ([Mendes et al., 2021](#)), and in order to preserve the Stokes expansion structure of [Tung and Huang \(1985\)](#), we modify the Haring function:

$$\mathcal{H}_{\alpha,\gamma} = \exp \left[-2\alpha^2 \left(1 - 1.24\varepsilon\alpha + 1.09\varepsilon^2\alpha^2 \right)^\gamma \right] \quad \therefore \quad \mathbb{P}_{\alpha,\gamma} = \exp \left\{ -\frac{8}{\varepsilon^2} \left[\sqrt{1 + \varepsilon\alpha\mathcal{H}_0^{1/2}} - 1 \right]^2 \right\} \quad , \quad (8)$$

to obtain the Modified Rayleigh-Haring-Tayfun (MRHT) model. Figure 2 shows that eq. (8) is much more flexible than [Haring et al. \(1976\)](#). However, the modified version of [Haring et al. \(1976\)](#) will violate the monotonicity of the exceeding probability ([Rohatgi, 1976](#)) and corollaries ([Mendes, 2021](#)), thus, we shall attempt to find a remedy for anomalies that may arise.

3. Tracking γ

In order to assess the validity of eq. (7) regarding the parameter γ we need to find clues on how to express it in terms of the given sea parameters in eq. (4). According to Figure 16 in [Mendes et al. \(2021\)](#), a combination of high

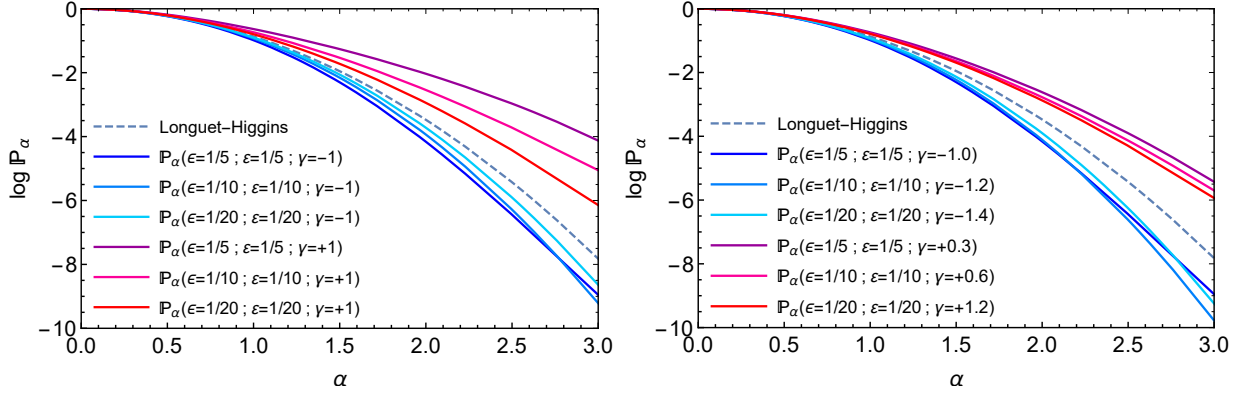


Figure 3: The inspection of Figure 16 in Mendes et al. (2021) according to the MRHT model with (left) increasing absolute values of (ϵ, ε) with fixed γ in groups of fixed ratio ε/ε and (right) a tentative change in γ to make each group have negligible variation.

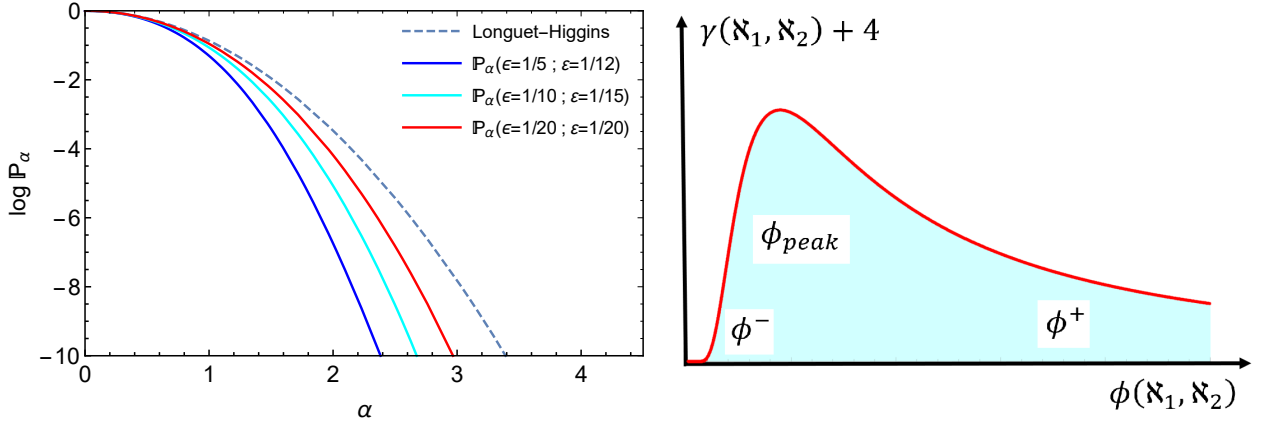


Figure 4: (Left) Testing of Mendes et al.'s Figure 16 according to the MRHT model with increasing absolute values of (ϵ, ε) and ratio ε/ε with fixed $\gamma = -2$ and (Right) Sketch of the function $\gamma = \gamma(\mathfrak{N}_1, \mathfrak{N}_2)$.

steepness and high height-to-depth ratio should lead to low probability. Likewise, a combination of low ε and low ϵ should return the very same outcome. That is because at fixed *nonlinearity* $\eta_{1/3}$, according to Table 4 of Mendes et al. (2021) we may use the approximation $\ln \mathbb{P}_\alpha \sim \varepsilon/\epsilon$ for qualitative analysis. However, as expected, Figure 3 shows this picture to not be too simplistic as described in the aforementioned table. We clearly see that when the probability will give skewed behavior depending on the sign of γ , thus suggesting that if $\gamma = \gamma(\phi)$, with an unknown function of sea parameters ϕ , given the central spot $\gamma(\phi_c) := 0$, we see that the γ function is skewed towards positive increments of ϕ_c . Therefore, whatever γ may be, a large deviation from $\gamma(\phi_c)$ will affect the exceeding probability significantly with fixed (ϵ, ε) . Now, according to Table 4 and Figure 11 of Mendes et al. (2021), the mediator when the latter two parameters are fixed is the *nonlinearity* $\eta_{1/3}$, hence, $\gamma = \gamma(\phi(\eta_{1/3}))$. For further validation of this hypothesis, Figure 4 (left) confirms that when γ , and thus $\eta_{1/3}$, is fixed, the higher the ratio ε/ϵ the higher the probability. At least theoretically, the MRHT model prescribes the exact same solution as the graphical description of Mendes et al. (2021): higher significant steepness and lower height-to-depth ratio increases the probability while the inverse decreases the probability, which also means that for fixed $\eta_{1/3}$ this produces a lower \mathfrak{N}_1 and by extension, lower \mathfrak{N}_2 . Thus, one can show that the Ursell number depends on these two parameters (see parameter definitions in Mendes et al. (2021)):

$$\text{Ur} \equiv \frac{6H_{1/3} \langle \lambda_{1/3} \rangle^2}{31\pi^2 D^3} \equiv \frac{6\langle \epsilon \rangle^3}{31\pi^2 \varepsilon^2} = \frac{6\eta_{1/3}^2 \langle \lambda_{1/3} \rangle}{31\pi^2 D} \cdot \mathfrak{N}_1 \mathfrak{N}_2 \equiv \frac{6\eta_{1/3}^2 \langle \epsilon \rangle}{31\pi^2} \cdot \mathfrak{N}_1^2 \quad . \quad (9)$$

Then, at fixed \mathfrak{N}_1 , we conclude that the Ursell number will increase, thus, Figure 3 (right) has identical probabilities if γ decreases when $\phi > \phi_c$ or γ increases when $\phi < \phi_c$, suggesting a bell curve centered at ϕ_c . Moreover, for the same

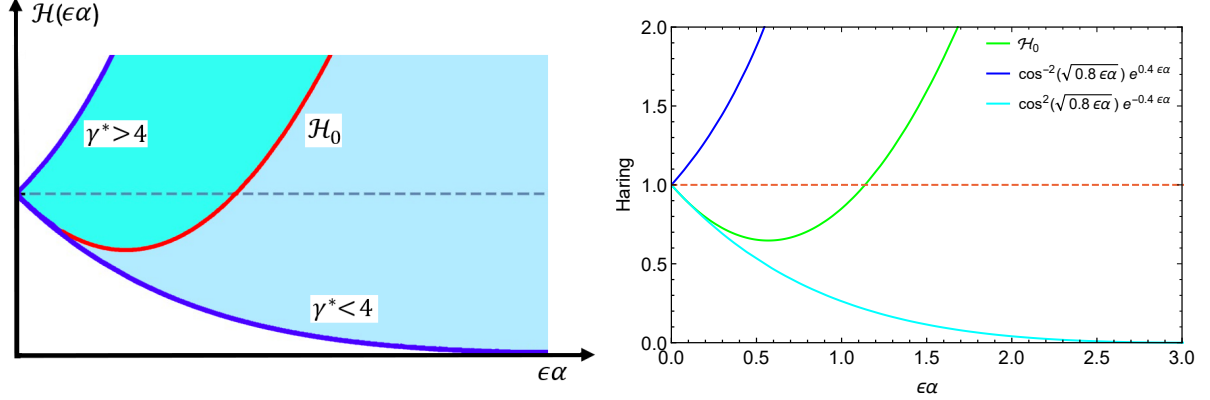


Figure 5: (Left) Sketch of Haring et al.'s root function and the necessary adjustments to the factor $\gamma = \gamma^* - 4$ and (Right) tentative numerical approximation for the sketch and $\mathcal{H}_0(\epsilon\alpha)$.

variation in ϵ we see that the region $\phi > \phi_c$ has a much faster drop $\Delta\gamma \sim -0.9$ than its counterpart $\phi < \phi_c$ increase $\Delta\gamma \sim +0.4$, producing a negative skewness. Nevertheless, the interval $\phi \in [\phi_c, +\infty)$ is of the order of its equivalent $\lambda_2/D \in [5, +\infty)$, such that the seemingly slow decay in the region $\phi \in [0, \phi_c)$ is actually much faster because it covers a very small interval $\lambda_2/D \in [0, 5)$. Therefore, we may describe, asymptotically, the shape of $\gamma(\phi)$ as follows, depicted in Figure 4 (right) and in agreement with Table 4 of Mendes et al. (2021):

$$\gamma(\phi(\mathfrak{N}_1^{(low)}, \mathfrak{N}_2^{(low)})) < \gamma(\phi(\mathfrak{N}_1^{(high)}, \mathfrak{N}_2^{(high)})) < \gamma(\phi(\mathfrak{N}_1^{(low)}, \mathfrak{N}_2^{(high)})) \quad . \quad (10)$$

Consequently, at fixed (ϵ, ε) , the effort of the system to produce shallow water rogue waves should be in general, but not always, much higher than for upper deep waters. Moreover, one may convince oneself that we need a translation for the nonlinear measure $\gamma^* \rightarrow \gamma + k$ in order to maintain a Gaussian shape (where k is some real non-negative number), due to the fact that γ is typically negative and barely crosses to the positive realm. A quick back-of-the-envelope reverse calculation using eq. (7) and the entries of Tables 1 and 3 of Mendes et al. (2021) will show that the interval of interest here is $-2 < \gamma < 1/2$, hence, $k = 4$ is advised to obtain a mathematical expression as simple as possible.

4. Modified Haring Function and a Constrained MRHT Model

Since we understand the rough shape of γ , we can apply the monotonicity condition to eq. (8), i.e. guaranteeing that the derivative of the exceeding probability is non-positive, which is reduced to:

$$\frac{d}{d\alpha}(\ln \mathcal{N}_\alpha) = \frac{8\mathcal{H}_0^{\gamma/2}}{\varepsilon} \left[1 - \frac{1}{\sqrt{1 + \varepsilon\alpha\mathcal{H}_0^{\gamma/2}}} \right] \left[1 + \frac{\alpha\gamma}{2\mathcal{H}_0} \frac{d\mathcal{H}_0}{d\alpha} \right] \geq 0 \quad . \quad (11)$$

Considering that the Haring function is strictly non-negative (see eq. (2)), we require:

$$1 + \frac{\alpha\gamma}{2\mathcal{H}_0} \frac{d\mathcal{H}_0}{d\alpha} \geq 0 \quad \therefore \quad \frac{\alpha}{\mathcal{H}_0} \frac{d\mathcal{H}_0}{d\alpha} \geq -\frac{2}{\gamma} \quad , \quad \forall \gamma \in \mathbb{R}^* \quad . \quad (12)$$

We should, however, be even more careful, and seek the conditions below:

$$\frac{d\mathcal{H}_0}{d\alpha} \geq 0 \Leftrightarrow \gamma \geq 0 \quad ; \quad \frac{d\mathcal{H}_0}{d\alpha} < 0 \Leftrightarrow \gamma < 0 \quad , \quad (13)$$

even though one finds the original condition already sufficient. As shown in Figure 5, the Haring function has both negative and positive slopes, with the latter dominating past $\epsilon\alpha \sim 0.5$ (see eq. (2)), though obeying eq. (12) when

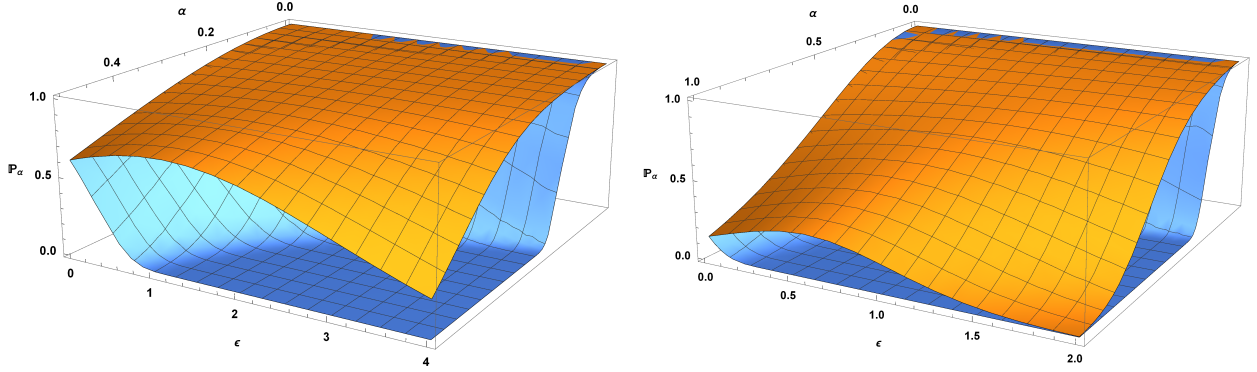


Figure 6: 3D plot of the old (yellow) and the new version of Haring et al.'s distribution through eq. (14). Notice that Haring et al. (1976) violates the depth-limited wave breaking section 4 of Mendes et al. (2021) by assigning a probability of 65.4% of finding wave heights $H_{1/3} > 2D$ for any dimensionless height $\alpha > 1/2$. The new model (blue) estimates the probability for the same scenario to be of the order of 10^{-46} . In this plot we used $\gamma \approx -4$ for very deep water waves, in accordance with figure 4. Likewise, on the right, the old version predicts an exceeding probability of nearly 20% of waves taller than $H_{1/3}$ with $H_{1/3} > D$ whilst the new model assigns a probability of 10^{-183} .

γ is not too negative, it can never satisfy the more strict condition of eq. (13). Therefore, instead of constraining the strength of the "meandering", we rather reformulate the Haring function to obey eq. (13). Hence, our task is to obtain a Taylor series capable of approximating the Haring function for $\epsilon\alpha < 0.5$ and departing from it to both vanishing ($\gamma < 0$) and divergent ($\gamma > 0$) regimes in Figure 5 (left). Clearly, the best option for a Taylor series obeying such constraints are of trigonometric behavior coupled to an exponential. Furthermore, the product of cosine and exponential functions feature an expansion (up to coefficients) of the type $1 - O(x) + O(x^2) + \dots$, being optimal for the modelling and generalization of eq. (2) and without undesirable trigonometric bouncing features. If, for the sake of simplicity, we rewrite (8) with 2γ , we obtain

$$\mathcal{H}_{0,\gamma} = \left[\cos^{-2|\gamma|} \left(\sqrt{0.8\epsilon\alpha} \right) e^{0.4\epsilon\alpha|\gamma|} \right]^{1/\gamma}, \quad \forall \gamma \in \mathbb{R}, \quad (14)$$

which is plotted in Figure 5 and matches the desired shape required by eq. (13). In addition, the new formulation (14) does not assign finite exceeding probability for extreme values of $\epsilon\alpha$ that would ultimately violate the ϵ bound, as shown by Figure 6. Hence, possessing all the mechanisms necessary to repair (7), we rewrite the new exceeding probability as:

$$\mathbb{P}_\alpha(\epsilon, \epsilon, \gamma^*) = \exp \left\{ -\frac{8}{\epsilon^2} \left[\sqrt{1 + \frac{\epsilon\alpha e^{2|\gamma^*-4|\epsilon\alpha/5}}{\cos^{-2|\gamma^*-4|}(\sqrt{4\epsilon\alpha/5})}} - 1 \right]^2 \right\}. \quad (15)$$

Following the reasoning of the previous section, we start with the idea of γ^* that is a function of \aleph_1 and \aleph_2 . For instance, low intermediate water waves are approximately described by $\aleph_1\aleph_2 \approx 40$ Ur. Tentatively, one can easily find a mathematical range for a good filter ϕ and thus fitting of the data, however, the filter should be obtainable from the Ursell number at leading order. Then, if we reverse engineer the entries of Tables 1 and 3 of Mendes et al. (2021) while combining eqs. (15) and (9), the most suitable clustering that makes the data as homogeneous as possible function $\gamma(\phi)$ is:

$$\gamma^*(\alpha, \phi) := \left(\frac{121}{6\alpha} \right)^{3/5} \frac{\phi^{-(68\alpha/33)^{5/7}}}{(e^{1/\phi} - 1)}, \quad \phi(\aleph_1, \aleph_2) = \frac{0.305}{\eta_{1/3}^4} (1 + \aleph_1)^{7/4} (1 + \aleph_2)^{7/4}. \quad (16)$$

Moreover, we introduce the error range for the calibration of γ^* in order to get a closer fit to the expected values of the latter that are not well covered by (16). Hence, we have:

$$\gamma^*(\alpha, \phi) \pm \Delta\gamma^* = \left(\frac{121 \pm 3\alpha}{6\alpha} \right)^{3/5} \frac{\phi^{-(68\alpha/33)^{5/7}}}{(e^{1/\phi} - 1)}. \quad (17)$$

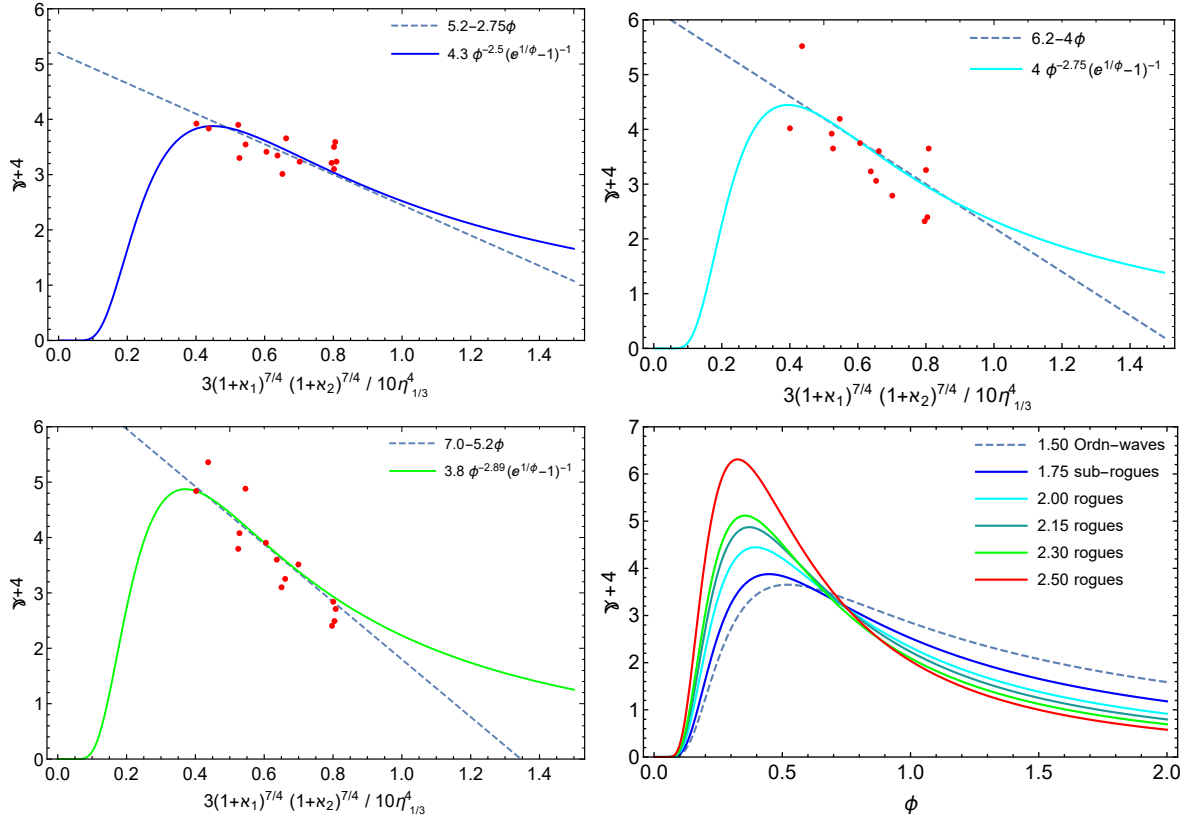


Figure 7: Calibration of eq. (15) through the required γ (red dots) for reproducing Mendes et al.'s statistics with respective colors from (Bottom Right) the model of $\gamma^*(\alpha, \aleph_1, \aleph_2)$ using eq. (16).

As a bonus, as shown in Figure 7, ϕ does such a good job at gathering homogeneously the γ extracted from Table 1 in Mendes et al. (2021), that is also possible to find a generalized expression for $\gamma^*(\alpha, \aleph_1, \aleph_2)$ conveying a linear model. However, our task is to provide a model that supports the interpretation of the underlying dynamics as suggested by Table 4 of Mendes et al. (2021) and all the constraints and conditions thereof, in addition to the interpretations and predictions of section 4 of Mendes et al. (2021). For instance, a linear γ model would make the distribution have a maximum in large depths (or small wavelengths) deep water and be infinitely negative for shallow, thus making it impossible to form rogue waves. Thence, for the reasons already pointed out by eq. (10) and in Figure 4, we select the model of eq. (16), whose non-trivial shape is depicted in Figure 8 (left). Generally, as conveyed by previous versions of \mathbb{P}_α (7, 8, 15), an α approaching zero should obtain a 100% of exceeding probability as attested by Longuet-Higgins (1952). Likewise, we need to find the limit of \mathbb{P}_α in eq. (15) when γ^* is very large. First, however, we remind the reader that:

$$\lim_{\substack{\alpha \rightarrow 0 \\ \gamma^* \rightarrow +\infty}} \gamma^* \cdot \alpha \approx O(\alpha^{2/5}) = 0 \quad . \quad (18)$$

Ergo, applying (18) into (15), we readily conclude:

$$\lim_{\substack{\alpha \rightarrow 0 \\ \gamma^* \rightarrow +\infty}} \mathbb{P}_\alpha(\gamma^*) \approx \exp\left\{-\frac{8}{\varepsilon^2} \left(\frac{\varepsilon\alpha}{2}\right)^2\right\} \approx e^{-2\alpha^2} = 1 \quad , \quad (19)$$

Thus being consistent with the standard limit of \mathcal{R}_α when α approaches zero, proving another advantage of using the modified Haring function of eq. (14) instead of eq. (2).

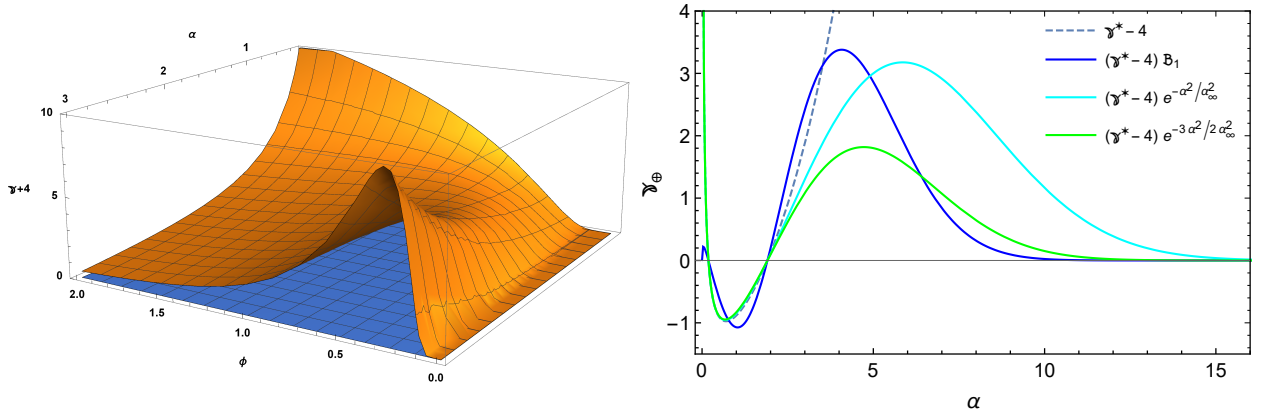


Figure 8: (Left) 3D plot of γ^* function of eq. (16) with varying dimensionless heights ($1/3 \leq \alpha \leq 3$) and the auxiliary parameter ϕ ($\mathcal{S}_1, \mathcal{S}_2$) and (Right) Damping of γ_\oplus for the storm 172. The upper bound for the storm is $\alpha_\infty = 4.72$. The simpler modification quickly departs from eq. (16) for mid-range α whereas the full modification reaches its peak before α_∞ .

4.1. Smoothness near α_∞

Nevertheless, we still need to obtain a bound for the specific case of very large dimensionless wave heights and obey the monotonicity condition (Mendes, 2021). This bound is also related to the first part of condition (4). The main issue at hand is that it is typically very complicated to satisfy the monotonicity and non-negative second derivative (henceforth called "meandering") simultaneously. Often distributions obey one and not the other. Moreover, the second derivative would look terribly complicated in eq. (13). Instead of finding a general formula for \mathcal{H}'_0 obeying monotonicity and "meandering" at once, it seems more realistic to stick to the general solution for monotonicity and modify it with a truncation that makes the "meandering" arise for selected storms. In other words, it might be too complicated to find a "meandering" formula for all storms, and even doing so, this expression would not affect the less complex form of eq. (24). Lastly, we notice that the meandering for small negative values of γ starts about or after its bound α_∞ (Mendes, 2021), whereas when feasible, the "meandering" should happen in the vicinity but not after its upper normalized height bound. Accordingly, when the normalized height approaches α_∞ the corresponding value of γ^* must drop, because eq. (13) at a very large γ requires a very high slope for \mathcal{H}_0 capable of producing Planck scale low probabilities (see Figure 6). However, this drop can not change the sign of γ , in order to not violate the meandering condition, such that this modification should be as shown in Figure 8 (right). Notice that at $\alpha > \alpha_\infty$ will reduce the distribution to the Tayfun (1980) form, however, at so large normalized heights it also produces Planck scale low likelihoods as required by eq. (1). Noticeably, the same work could be obtained by making γ to flatten out at $\alpha \sim \alpha_\infty$ and then grow again at $\alpha > \alpha_\infty$, producing likelihoods as low as in Figure 6, however, the modification for γ would be even more burdensome. These considerations are important for super-rogue waves and the "meandering". Using the four storms with highest rogue wave occurrence and eq. (4) as *liaisons*, we modify γ :

$$\mathfrak{B}_1 := \frac{\gamma_\oplus}{\gamma} = \frac{\tanh\left(\frac{\xi^2 \alpha}{6\phi^3 \alpha_\infty}\right) \cdot \exp\left[-4 \frac{\alpha_\infty^{2/40}}{\alpha_\infty^2} \frac{\alpha^2}{\alpha_\infty^2}\right]}{\tanh\left[\frac{2\alpha_\infty}{2\alpha + 25\alpha_\infty^2 (\ln \xi)^3}\right]}, \quad (20)$$

Where ξ denotes the bound availability, i.e. how the combined typical maximum normalized heights α_\star and $\|\epsilon\alpha\|_\infty/\epsilon$ measure up the upper bound α_∞ . Therefore, we obtain,

$$\xi := \alpha_\infty \sqrt{\frac{\epsilon}{\alpha_\star \|\epsilon\alpha\|_\infty}} = \frac{16}{7} \alpha_\infty \langle s_s \rangle \cdot \left[\frac{\lambda_2}{D} + 4 \tanh\left(\frac{2\pi D}{\lambda_2}\right) \right]^{1/2}. \quad (21)$$

In Figure 8 (right) we show the differences between models (16) and (20): the first sharply increases in the vicinity of α_∞ whereas the second maintains a stable trajectory of small values for γ_\oplus . From Figure 9 (right) the roles played by each parameter becomes clear: ξ controls the strength of the meandering, ϕ controls the sign of γ and also affect

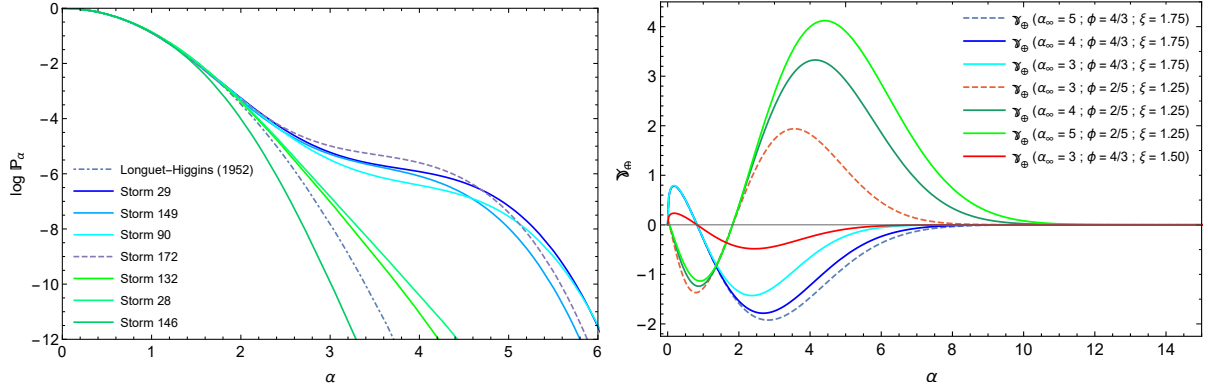


Figure 9: (Left) Probability model variability for the storms in Mendes et al. (2021) due to (ϕ, ξ) with modified $\gamma_{\oplus} = \gamma\mathfrak{B}_1$ and $\mathfrak{B}_2^{\infty} = 2$ and (Right) deep and shallow water wave regimes using their characteristics ϕ and attached to upper bounds α_{∞} .

ξ strength (because shallow water waves with higher ξ still produced a smaller $\Delta\gamma$ than a deep water counterpart), while an increasing α_{∞} diminishes the likelihood (if everything in eq. (15) is fixed except γ), as per condition (13) a more positive γ is attached to a positive slope \mathcal{H}_0 producing very low probabilities and vice-versa, partially explaining why the storms with highest (on average) bounds α_{∞} on Table 5 of Mendes et al. (2021) are those with the smallest ratio $\|\alpha\|/\alpha_{\infty}$. This interpretation is also roughly supported by our conjectures in sections 5.3.2 and 5.5 in Mendes et al. (2021), as when α_{∞} increases due to an increase in $\langle\langle\delta_2\rangle\rangle$, a decrease in \mathbb{E}_{α} follows. Notably, the "meandering" strength due to ξ is also corroborated by Figure 9 (left): When $\phi \sim \phi_c$, e.g. the peak of γ , a higher bound availability will produce higher distributions until it finally creates the "meandering". However, the tipping point towards the "meandering" will depend on $(\eta_{1/3}, \epsilon, \varepsilon)$ altogether. As expected, when ξ is smaller, the meandering does not happen, with a further observation that variations in ϕ seem to be symmetrical both to γ_{\oplus} and RD. Note, however, that Figure 9 (right) is a function of α and not ϕ as in Figure 4 (right). Lastly, it is important to note that if $\mathfrak{B}_1 \sim e^{-\alpha^2/\alpha_{\infty}^2}$ we would produce very similar results, leading to the same conclusion that a smaller bound α_{∞} would produce a stronger lowering of $\gamma(\alpha)$, and thus, producing a "meandering" and possibly avoiding overthinking for any qualitative analysis. On the other hand, the more complex function $\mathfrak{B}_1(\xi)$ brings in richer interpretation, which validates its choice. A further modification of interest, but not necessarily mandatory if we use $\mathfrak{B}_1 \sim e^{-\alpha^2/\alpha_{\infty}^2}$, is related to the exponent of the trigonometric function that is a Taylor expansion of Haring et al. (1976) in eq. (15). The new exponent shall read (see Figure 10, left):

$$\mathfrak{B}_2 := 2 + \frac{7\alpha_{\infty}}{8\alpha\xi} \cdot \tanh\left(\frac{7\alpha_{\infty}}{8\alpha\xi}\right) \left[1 + e^{(\alpha_{\infty}-\alpha)/\xi}\right]^{-1} . \quad (22)$$

The main effect of \mathfrak{B}_2 is to enhance the cosine exponent in the vicinity of the bound α_{∞} without affecting the bulk waves significantly. Furthermore, very high bound availability is counter-productive towards \mathfrak{B}_2 , thus creating a balance between \mathfrak{B}_1 and \mathfrak{B}_2 contributions.

Overall, the uneven occurrence of rogue waves is mostly due to a strong variation in γ when variations in ϵ and ε are small, such as in Mendes et al. (2021). This can be seen in 7 as the variations in γ to produce the same probability narrows as α decreases. In this sense, in agreement with the interpretation of Mendes et al. (2021), a better rogue wave definition would be one in which the storm parameters influence on γ grows considerably. Moreover, we observe a tendency of higher rogue wave occurrence in deep and intermediate water waves for small $\eta_{1/3}$. In other words, it is easier for γ to reach high non-negative values when $\phi < 1$. Accordingly, typical shallow water waves with $\langle\epsilon\rangle \approx 1/5$ tend to have high occurrence of rogue waves if the following holds:

$$\frac{3}{10\eta_{1/3}^4} \left(1 + \frac{30}{\eta_{1/3}}\right)^{7/4} \left(1 + \frac{1}{5\eta_{1/3}}\right)^{7/4} \sim 1 \quad \Leftrightarrow \quad \eta_{1/3} \sim 2.4 \quad , \quad (23)$$

thus, the "meandering" in shallow water would require a herculean effort from the system to form rogue waves. On other hand, through a proper combination of ϵ and ε is possible to form rogue waves in shallow water, though is

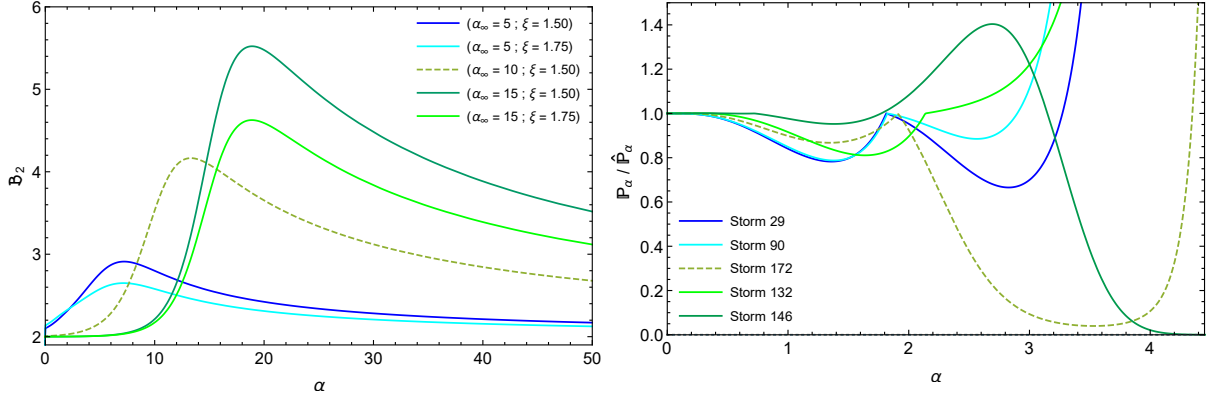


Figure 10: (Left) Revisited function in eq. (15) with varying normalized height and bound availability and (Right) ratio of the distributions in eqs. (15) and (24). For the majority of storms the simpler model is sufficient for an accurate analysis of rogue wave occurrence when $2 \leq \alpha \leq 2.3$.

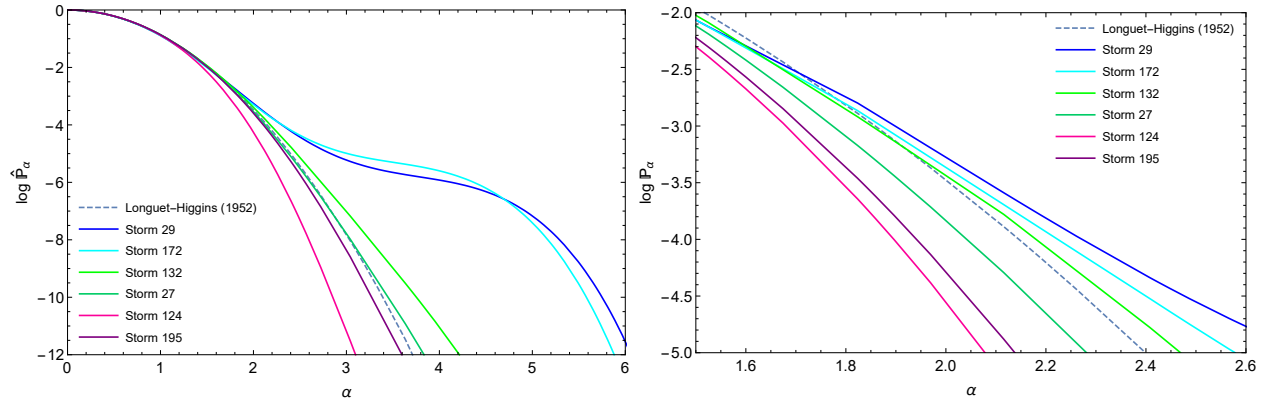


Figure 11: Predicted uneven distribution among storms (Stansell, 2004) with Sub-Rayleigh and Super-Rayleigh regimes for both models in eq. (25).

unlikely to form as many rogue waves as in deep water. Therefore, the consequences arising from the present model are in complete agreement with available in-situ data and numerical simulations (Glukhovskii, 1966; Bitner, 1980; Chien et al., 2002; Didenkulova and Anderson, 2010; Didenkulova and Rodin, 2012; Barbariol et al., 2015).

5. Ultimate RHT Model

Combining the previous sections, the final version of the exceeding probability reads:

$$\hat{P}_\alpha(\eta_{1/3}, \epsilon, \varepsilon) = \exp \left\{ -\frac{8}{\varepsilon^2} \left[\sqrt{1 + \frac{\varepsilon \alpha e^{2|\gamma|\varepsilon \mathfrak{B}_1/5}}{\cos^{-|\gamma|\mathfrak{B}_2}(\sqrt{4\varepsilon \alpha/5})}} - 1 \right]^2 \right\}, \quad (24)$$

Where γ , \mathfrak{B}_1 and \mathfrak{B}_2 are also functions of $\eta_{1/3}$, ϵ and ε , due to eqs. (16), (17), (20) and (22). Hence, the final picture for the exceeding probability proposed is (P_α as in eq. (15))

$$\mathbb{P}(H > \alpha H_{1/3}) = \begin{cases} \hat{P}_\alpha \Leftrightarrow \left| 1 - P_\alpha / \hat{P}_\alpha \right| > \frac{1}{4} & , \alpha \in]2, +\infty[\\ P_\alpha \Leftrightarrow \left| 1 - P_\alpha / \hat{P}_\alpha \right| \leq \frac{1}{4} & , \alpha \in]2, +\infty[\\ \hat{P}_\alpha \Leftrightarrow \phi \xi \geq \frac{3}{4} \alpha & , \alpha \in [1.5, 2] \\ P_\alpha \Leftrightarrow \phi \xi < \frac{3}{4} \alpha & , \alpha \in [1.5, 2] \end{cases}. \quad (25)$$

ID	$\alpha > 1.75$	$\alpha > 2$	$\alpha > 2.5$	$\alpha > 3$
29	30 (31 ± 2)	12 (7.2 ± 0.5)	0 [0.5 ± 0.1]	0 [0.05 ± 0.02]
149	95 (100 ± 14)	26 (23.6 ± 1.8)	1 [1.6 ± 0.6]	0 [0.18 ± 0.09]
90	111 (103 ± 9)	20 (23.3 ± 1.2)	1 (1.1 ± 0.2)	0 [0.09 ± 0.03]
172	54 (49 ± 6)	9 (11.0 ± 0.8)	1 [1.0 ± 0.3]	1 [0.17 ± 0.14]
132	68 (81 ± 7)	14 (14.2 ± 2.2)	0 (0.3 ± 0.1)	0 [0.00 ± 0.00]
28	30 (47 ± 5)	6 (9.7 ± 0.5)	0 [0.2 ± 0.1]	0 [0.00 ± 0.00]
146	20 [17 ± 2]	4 (1.6 ± 0.2)	0 [0.0 ± 0.0]	0 [0.00 ± 0.00]
23	42 (32 ± 4)	5 (4.3 ± 0.9)	0 [0.1 ± 0.1]	0 [0.00 ± 0.00]
26	33 (47 ± 4)	4 (7.2 ± 0.1)	0 [0.1 ± 0.1]	0 [0.00 ± 0.00]
127	15 (14 ± 1)	2 (1.2 ± 0.2)	0 [0.0 ± 0.0]	0 [0.00 ± 0.00]
25	21 (26 ± 3)	2 (4.0 ± 0.9)	1 [0.1 ± 0.1]	0 [0.00 ± 0.00]
27	23 (25 ± 3)	1 (3.0 ± 0.6)	0 [0.0 ± 0.0]	0 [0.00 ± 0.00]
124	30 [20 ± 2]	0 (0.6 ± 0.2)	0 [0.0 ± 0.0]	0 [0.00 ± 0.00]
195	9 (7 ± 1)	0 (0.5 ± 0.1)	0 [0.0 ± 0.0]	0 [0.00 ± 0.00]
Σ	581 (590 ± 63)	105 (111.4 ± 11.1)	4 [5.0 ± 1.4]	1 [0.49 ± 0.26]
\mathcal{R}_α	774	119	1	0

Table 1: Predicted values for the entries of Table 1 in [Mendes et al. \(2021\)](#) from our model \mathbb{P}_α (15) inside round brackets and $\hat{\mathbb{P}}_\alpha$ (24) with square brackets. The proposed model clearly outperforms [Longuet-Higgins](#)'s distribution for a variety of normalized heights. Out of the 60 total entries of this table, [Longuet-Higgins](#)'s distribution accurately predicts about 40% while the MRHT model accurately predicted 75% of them, whereas the (15) model has nearly 70% of accuracy. Considering only the first two columns (with higher statistical significance), these accuracy percentages are reduced to 25% and 70% respectively.

These conditions on the distribution choice seems to be a sort of phase transition. According to Figure 10, the models \mathbb{P}_α (15) and $\hat{\mathbb{P}}_\alpha$ (24) are nearly indiscernible for the majority of storms in the interval $0 < \alpha \leq 2$, and indeed the model (15) is quite reliable when $1.50 < \alpha < 2.25$, showing very few exceptions to this rule. However, their range of similarity is affected by sea parameter variations, as shown by the very same plot. Therefore, as Figure 11 shows, our final model matches these qualitative observations of uneven occurrence, variability (or stratification) of the probability distribution as well as the super-rogue wave "meandering".

5.1. Overall Assessment

Most models focus on either explaining the geometry of the tallest wave in a storm (such as the Draupner wave) or to predict accurate ocean wave statistics for fixed $\alpha = 2$. Our model in eq. (25) intends to be a good mathematical description for the entire interval $\alpha \in [1, \alpha_\infty)$. As such, Table 1 shows the remarkable performance of eq. (25) across four crucial fixed normalized heights, including [Longuet-Higgins \(1952\)](#) for the total count only (see Table 2 of [Mendes and Scotti \(2020\)](#) for its individual performance). Contrary to [Longuet-Higgins \(1952\)](#), our model maintains an error smaller than 20% in virtually all cases and smaller than 10% in half of all cases.

5.1.1. Super-rogue Wave Assessment

Despite several wave tank experiments and field observations published in the literature, most reports do not mention a wave with a normalized height of $\alpha > 3$ (hence called super-rogue waves), deserving special consideration. The most studied individual rogue waves, the Draupner wave ([Haver and Andersen, 2000](#); [Øistein, 2002](#); [Haver, 2004](#); [Walker et al., 2004](#); [Adcock et al., 2011](#); [Clauss and Klein, 2011](#); [Adcock, 2017](#)) and the Andrea Wave ([Magnusson and Donelan, 2013](#); [Cherneva and Guedes Soares, 2014](#); [Bitner-Gregersen et al., 2014](#); [Donelan and Magnusson, 2017](#); [Fedele et al., 2017](#)) are well below this threshold. The characteristics of [Stansell](#)'s super-rogue wave are much more remarkable than the famous Draupner and Andrea waves, as shown by Table 2. Applying the available data of storm 172 found in Table 3 of [Mendes et al. \(2021\)](#) into (16), we obtain the storm average $\phi_{172} \approx 0.523$. According to the conditions laid in eq. (25), we reevaluate the North Alwyn super-rogue wave minimum return period, obtaining 65,000 waves (6 days), equivalently a likelihood of 10^{-5} . As the storm 172 contains 23,591 waves (2 days and 4 hours), we obtain a maximum relative probability of 36% to find at least one super-rogue wave as reported by [Stansell](#)

<i>Observation</i>	$H_{1/3}$ (m)	$\lambda_{1/3}$ (m)	T_z (s)	H (m)	$H/H_{1/3}$	\mathcal{Z}_c	$\mathcal{Z}_c/\mathcal{Z}_t$	$\mathcal{Z}_c/H_{1/3}$
Draupner	11.92	≈ 326	11.20	25.01	2.098	18.49	2.84	1.55
Andrea	9.18	≈ 212	9.02	21.14	2.303	14.97	2.43	1.63
Alwyn	5.64	≈ 179	8.18	18.04	3.190	13.90	3.36	2.46

Table 2: Observations at depths of 130m, 130m and 70m (Magnusson and Donelan, 2013).

(2004). Notice, however, that using $\mathfrak{B}_1 \sim e^{-\alpha^2/\alpha_\infty^2}$ would make this likelihood increase to 70-80% while not affecting lower statistics ($\alpha < 2.5$), being disfavored not on numerical grounds, but rather on the lack of physical interpretations for this model.

On the other hand, more established distributions discussed in Mendes et al. (2021) would prescribe the respective likelihoods for the North Alwyn super-rogue wave: $e^{-2(3.19)^2} \sim 10^{-9}$ (Longuet-Higgins, 1952), $4 \cdot 10^{-8}$ (Haring et al., 1976), $3 \cdot 10^{-12}$ (Forristall, 1978), $8 \cdot 10^{-8}$ (Tayfun, 1980) and $3 \cdot 10^{-8}$ (Forristall, 2000). Looking from another perspective, we can analyze the likelihood for the North Alwyn wave by models of rogue wave crest exceeding probability. For instance, Longuet-Higgins’s crest model predicts a probability of $e^{-8(2.46)^2} \sim 10^{-21}$ for the North Alwyn super-rogue wave crest. Considering the storm zero-crossing period of 8 s, the latter estimates a necessary interval of $3 \cdot 10^{14}$ years for this wave to appear at a fixed point in the ocean, or ten thousand times the age of the universe. However, according to second-order models, the Draupner and Andrea wave crests should have an exceeding probability of $5 \cdot 10^{-7}$ (Øistein, 2002), $4 \cdot 10^{-6}$ (Prevosto and Bouffandeau, 2002), $5 \cdot 10^{-6}$ (Walker et al., 2004), $6 \cdot 10^{-7}$ (Forristall, 2005) and more recently $3 \cdot 10^{-6}$ (Adcock, 2017), whereas Longuet-Higgins’s would estimate $e^{-8(1.60)^2} \sim 10^{-9}$. On the other hand, the best estimate for Draupner and Andrea (Adcock, 2017) would likely assign an exceeding probability of 10^{-11} for the North Alwyn super-rogue wave height, the equivalent of 26,000 years.

6. Conclusions

Given the scope of this endeavor, a review of the results found in this paper are: the proposed exceeding probability is the first in the literature to combine three major sea state variables that are readily available from hindcast and that mathematically are implemented as three dimensionless variables ($\epsilon, \varepsilon, \eta_{1/3}$). Through a geometrically inspired model, we have obtained much better predictions than the most prestigious distributions in the literature as discussed in Mendes (2021). We have also implemented the relevant physical variables of ocean states of Mendes et al. (2021) into our distribution. It is also the first to introduce a probability distribution attached to an interpretation based on a the combination of these three dimensionless variables (as shown in figure 3 of Part I) while obeying all the bounds on $\alpha, \epsilon, \varepsilon$. Moreover, it shows unique flexibility (oscillation around the Longuet-Higgins (1952), the ”equilibrium” model) not found in any distribution from previous works. Additionally, our model prescribes an interpretation of the combination of sea state parameters that could be a blueprint for rogue wave warning systems. Furthermore, it does not depend heavily on skewness or kurtosis, which is the cause for turning Longuet-Higgins (1963) and similar models into cumbersome and numerically impractical models.

Contrary to other models, the new exceeding probability is generous to higher rogue waves ($\alpha \geq 3$) without having any anomalous behavior for other α , such as Gaussian shape for the return period. The major innovation of this work relies on the continuous approach to the exceeding probability distribution. In fact, we experimented the same model for seven different values of the dimensionless wave height α and have conclusively shown how sea states create variability in empirical distributions. Is important to note the remarkable accuracy of the presented model for waves that are nearly rogues: it was expected that Longuet-Higgins’s model would be the best approximation for bulk waves. Thought it wasn’t the original aim and scope of this work, improving the description of bulk waves by RD is certainly welcome and of good value.

Forristall’s respected second model predicts that storm 124 has the highest probability of featuring rogue waves (Mendes et al., 2021), as it has the highest steepness. In practice, this storm had no rogue wave and its return period for sub-rogue waves is also higher than predicted by Longuet-Higgins (1952). On the other hand, Forristall (2000) predicts a range of variability for the return period of all fourteen storms to be $\mathcal{N} \in [1046, 1500]$, more than two times lower than Longuet-Higgins’s prediction, thus predicting 22 rogue waves for storm 124 alone. Accordingly,

Forristall (2000) would foresee nearly 300 rogue waves appearing in the fourteen storms, almost three times the number reported by Stansell (2004). Therefore, second-order models (theoretical, numerical and experimental) do not produce uneven extreme wave distributions as observed in Stansell (2004). Moreover, additional distributions showed no mathematical or numerical advantage in both fitting the rogue wave uneven occurrence and explaining the source of this phenomenon, such as Naess (1985), Boccotti (1989), Tayfun (1990), Tayfun and Fedele (2007), Boccotti (2000) (see Mendes et al. (2021) for a review).

Additionally, Barbariol et al. (2015) reports a study of metocean forcings on the maximum of the extreme wave crests and demonstrated that depth-induced shoaling significantly decreased the maximum extreme wave crest, thus implying that shallow water wave regime has lower probability of exceeding the rogue wave threshold, i.e. the shape of γ . Moreover, it was also found that a current in opposition to wave train would increase the exceeding probability, however, the increase in extreme wave crest was only of 4% with an opposing current with velocity of 0.4 m/s at the surface. Comparing it to the Agulhas current that has a velocity of 2.1 m/s at the surface (Boebel et al., 2003), the maximum increase of a extreme wave crest due to an opposing current would be of the order of 20%. Such an increase is not enough to explain for example the North Alwyn super-rogue wave crest which is about 80% taller than expected by Longuet-Higgins (1952).

Despite the remarkable success of both interpretative and predictive branches of the proposed model with physical bounds laid down in Mendes et al. (2021), our model is vulnerable to large deviations from the average values of $\eta_{1/3}$, ϵ and ε , as already expected in the storm geometry discussion from Mendes et al. (2021). We suggest that a group of wave records should be combined and averaged-out and analyzed by eq. (15) if and only if the deviation of the significant wave height and other major variables does not exceed 25%. Higher deviations will likely increase the discrepancy between the prediction and observation of the return period of rogue waves and we believe that is the most probable cause of disagreement among many studies, in particular the very large deviation among samples as analyzed in Christou and Ewans (2014). Moreover, our model needs validation for upper intermediate and shallow water waves, since the available data was obtained for an average $\lambda_2 \approx 0.78D$. Another future work will deal with data having variations in water depth while maintaining the water wave regime. Finally, more data is needed for full validation of the simpler and the complex RHT models presented, but regardless of its validity to other data sets it represents a good toy model for explaining both underprediction and overprediction of the Longuet-Higgins's model and because its geometrical structure can be used for an ultimate generalization.

7. Acknowledgements

S.M. and A.S. were supported by the National Science Foundation under grant OCE-0729636.

References

- Adcock, T., 2017. A note on the set-up under the draupner wave. *J. Ocean Eng. Mar. Energy* 3, 89–94.
- Adcock, T., Taylor, P., Yan, S., Ma, Q., Janssen, P., 2011. Did the draupner wave occur in a crossing sea? *Proc. R. Soc. A* 467, 3004–3021.
- Akhmediev, N., Ankiewicz, A., Soto-Crespo, J.M., 2009a. Rogue waves and rational solutions of the nonlinear schrödinger equation. *Phys. Rev. E* 80, 026601.
- Akhmediev, N., Ankiewicz, A., Taki, M., 2009b. Waves that appear from nowhere and disappear without a trace. *Phys. Lett. A* 373, 675–678.
- Akhmediev, N., Korneev, V., 1986. Modulation instability and periodic solutions of the nonlinear schrödinger equation. *Theor. Math. Phys.* 69, 1089–1093.
- Al-Humoud, J., Tayfun, M., Askar, H., 2002. Distribution of nonlinear wave crests. *Ocean Eng.* 29, 1929–1943.
- Barbariol, F., Benetazzo, A., Carniel, S., Sclavo, M., 2015. Space-time wave extremes: The role of metocean forcings. *J. Phys. Oceanogr.* 45, 1897–1916.
- Bitner, E.M., 1980. Non-linear effects of the statistical model of shallow-water wind waves. *Applied Ocean Research* 2, 63–73.
- Bitner-Gregersen, E., Fernandez, L., Lefèvre, J., Monbaliu, J., Toffoli, A., 2014. The north sea andrea storm and numerical simulations. *Natural Hazards and Earth System Sciences* 14, 1407–1415.
- Bitner-Gregersen, E., Gramstad, O., 2015. Rogue waves: Impact on ships and offshore structures. DNV GL Strategic Research & Innovation Position Paper.
- Boccotti, P., 1989. On mechanics of irregular gravity waves. In: *Atti della ASccad. naz. dei Lincei* A386 19.
- Boccotti, P., 2000. *Wave mechanics for ocean engineering*. Elsevier Oceanography Series.
- Boebel, O., Rossby, T., Lutjeharms, J., Zenk, W., Barron, C., 2003. Path and variability of the agulhas return current. *Deep-Sea Res. II* 50, 35–56.
- Cherneva, Z., Guedes Soares, C., 2014. Time-frequency analysis of the sea state with the andrea freak wave. *Nat. Hazards Earth Syst. Sci.* 14, 3143–3150.
- Chien, H., Kao, C., Chuang, L., 2002. On the characteristics of observed coastal freak waves. *Coastal Eng.* 44, 301–319.

- Christou, M., Ewans, K., 2014. Field measurements of rogue water waves. *J. Phys. Oceanogr.* 9, 2317–2335.
- Cieslikiewicz, W., 1998. Maximum-entropy probability distribution of wind wave free-surface elevation. *Oceanologia* 40, 205–229.
- Clauss, G., Klein, M., 2011. The new year wave in a seakeeping basin: Generation, propagation, kinematics and dynamics. *Ocean Eng.* 38, 1624–1639.
- Cruz, A., Krausmann, E., 2008. Damage to offshore oil and gas facilities following hurricanes katrina and rita: An overview. *J. Loss Prev. Proc. Ind.* 21, 620 – 626.
- Davey, A., Stewartson, K., 1974. On three-dimensional packets of surface waves. *Proc. R. Soc. A* 338, 101–110.
- Dematteis, G., Grafke, T., Onorato, M., Vanden-Eijnden, E., 2019. Experimental evidence of hydrodynamic instantons: The universal route to rogue waves. *Phys. Rev. X* 91.
- Dematteis, G., Grafke, T., Vanden-Eijnden, E., 2018. Rogue waves and large deviations in deep sea. *Proc. Natl. Acad. Sci. USA* 115, 855–860.
- Didenkulova, I., Anderson, C., 2010. Freak waves of different types in the coastal zone of the baltic sea. *Nat. Hazards Earth Syst. Sci.* 10, 2021–2029.
- Didenkulova, I., Rodin, A., 2012. Statistics of shallow water rogue waves in baltic sea conditions: the case of tallinn bay. in: *Proc. of the 2012 IEEE/OES Baltic Int. Symposium*, 1–6.
- Donelan, M., Magnusson, A.K., 2017. The making of the andrea wave and other rogues. *Sci. Rep.* 7, 44124.
- Dysthe, K., 1979. Note on a modification to the nonlinear schrödinger equation for application to deep water waves. *Proc. R. Soc. A* 369, 105–114.
- Dysthe, K., Krogstad, H., Muller, P., 2008. Oceanic rogue waves. *Annu. Rev. Fluid. Mech.* 40, 287–310.
- Faukner, D., 2002. Shipping safety: A matter of concern. *Ingenia, The Royal Academy of Engineering, Marine Matters*, 13–20.
- Fedele, F., 2015. On the kurtosis of deep-water gravity waves. *J. Fluid Mech.* 782, 25–36.
- Fedele, F., Brennan, J., De Leon, S., Dudley, J., Dias, F., 2016. Real world ocean rogue waves explained without the modulational instability. *Sci. Rep.* 6, 27715.
- Fedele, F., Lugni, C., Chawla, A., 2017. The sinking of the el faro: Predicting real world rogue waves during hurricane joaquin. *Sci. Rep.* 7.
- Forristall, G., 1978. On the distributions of wave heights in a storm. *J. Geophys. Res.* 83, 2353–2358.
- Forristall, G., 2000. Wave crest distributions: observations and second order theory. *J. Phys. Ocean.* 30, 1931–1943.
- Forristall, G., 2005. Understanding rogue waves - are new physics necessary? *Proc. 14th Aha Huliko'a Winter Workshop*.
- Glukhovskii, B., 1966. Investigation of sea wind waves (in russian). *Gidrometeoizdat Publisher*.
- Haring, R., Osborne, A., Spencer, L., 1976. Extreme wave parameters based on continental shelf storm wave records. *Proc. 15th Int. Conf. on Coastal Engineering, Honolulu, HI*, 151–170.
- Haver, S., 2004. A possible freak wave event measured at the draupner jacket january 1 1995. *Proc. Rogue Waves 20-22 October IFREMER*.
- Haver, S., Andersen, O., 2000. Freak waves: Rare realizations of a typical population of typical realizations of a rare population? *Proc. 10th Int. Offshore Polar Eng. Conf. Seattle* 3, 123–130.
- Jahns, H., Wheeler, J., 1973. Long-term wave probabilities based on hindcasting of severe storms. *J. Petrol. Technol.* 25, 473–486.
- Janssen, P., 2003. Nonlinear four-wave interactions and freak waves. *J. Phys. Oceanogr.* 33, 863–884.
- Karmpadakis, I., Swan, C., Christou, M., 2020. Assessment of wave height distributions using an extensive field database. *Coastal Eng.* 157.
- Kharif, C., Pelinovsky, E., 2003. Physical mechanisms of the rogue wave formation. *Eur. J. Mech. B Fluids* 22, 603–634.
- Kobayashi, N., Herrman, M., Johnson, B., Orzech, M., 1998. Probability distribution of surface elevation in surf and swash zones. *Journal of Waterway, Port, Coastal and Ocean Engineering* 124, 99–107.
- Kriebel, U., Dawson, T., 1991. Nonlinear effects on wave groups in random seas. *Journal of Offshore Mechanics and Arctic Engineering* 113, 142–147.
- Krogstad, H., Barstow, S., 2004. Analysis and applications of second-order models for maximum crest height. *J. Offshore Mech. Arctic Eng.* 126, 66–71.
- Langley, R., 1987. A statistical analysis of non-linear random waves. *Ocean Eng.* 14, 389–407.
- Longuet-Higgins, M., 1952. On the statistical distribution of the heights of sea waves. *Journal of Marine Research* 11, 245–265.
- Longuet-Higgins, M., 1963. The effect of non-linearities on statistical distributions in the theory of sea waves. *J. Fluid Mech.* 17, 459–480.
- Magnusson, A.K., Donelan, M., 2013. The andrea wave characteristics of a measured north sea rogue wave. *J. Offshore Mech. Arctic Eng.* 135, 031108.
- Mallory, J., 1974. Abnormal waves in the south-east coast of south africa. *Int. Hydrog. Rev.* 51, 89–129.
- Mendes, S., 2021. Towards the unification of rogue wave statistics i: On the necessary response of distributions to sea state variables. *EarthArxiv*.
- Mendes, S., Scotti, A., 2020. Rogue wave statistics in (2+1) gaussian seas i: Narrow-banded distribution. *Appl. Ocean Res.* 99, 102043.
- Mendes, S., Scotti, A., Stansell, P., 2021. On the physical constraints for the exceeding probability of rogue waves in deep water. *EarthArxiv, to appear in App. Ocean Res.*
- Mori, N., Yasuda, T., 2002. A weakly non-gaussian model of wave height distribution random wave train. *Ocean Eng.* 29, 1219–1231.
- Naess, A., 1985. On the distribution of crest to trough wave heights. *Ocean Eng.* 12, 221–234.
- Ochi, M., 1986. Non-gaussian random processes in ocean engineering. *Probabilistic Engineering Mechanics* 1, 28–39.
- Ochi, M., Ahn, K., 1994. Probability distribution applicable to non-gaussian random processes. *Probabilistic Engineering Mechanics* 9, 255–264.
- Øistein, H., 2002. Statistics for the draupner january 1995 freak wave event. *Proc. Int. Conf. on Offshore Mechanics and Arctic Eng.* 2, 691–698.
- Onorato, M., Cavaleri, L., Fouques, S., Gramstad, O., Janssen, P., Monbaliu, J., Osborne, A., Pakozdi, C., Serio, M., Stansberg, C., Toffoli, A., Trulsen, K., 2009. Statistical properties of mechanically generated surface gravity waves: A laboratory experiment in a three-dimensional wave basin. *J. Fluid Mech.* 627, 235–257.
- Onorato, M., Residori, S., Bortolozzo, U., Montina, A., Arecchi, F., 2013. Rogue waves and their generating mechanisms in different physical contexts. *Phys. Rep.* 528, 47–89.
- Peregrine, D., 1983. Water waves, nonlinear schrödinger equations and their solutions. *J. Aust. Math. Soc. Ser. B* 25, 16–43.
- Prevosto, M., Bouffandeau, B., 2002. Probability of occurrence of a "giant" wave crest. *Proc. Int. Conf. on Offshore Mechanics and Arctic Eng.* 2, 483–490.
- Rohatgi, V., 1976. *An Introduction to Probability and Statistics*. Wiley, New York.

- Savina, H., Lefevre, J.M., Josse, P., Dandin, P., 2003. Definition of warning criteria. Proc. MaxWave Final Meeting .
- Socquet-Juglard, H., Dysthe, K., Trulsen, K., Krogstad, H., Liu, J., 2005. Probability distributions of surface gravity waves during spectral changes. *Journal of Fluid Mechanics* 542, 195–216.
- Song, J.B., Hou, Y.J., He, Y.J., Wu, Y.H., Yin, B.S., 2002. Statistical distribution of wave-surface elevation for second-order random directional ocean waves in finite water depth. *Coastal Eng.* 46, 51–60.
- Srokosz, M., 1998. A new statistical distribution for the surface elevation of weakly nonlinear water waves. *Journal of Physical Oceanography* 28, 149–155.
- Stansell, P., 2004. Distribution of freak wave heights measured in the north sea. *Appl. Ocean Res.* 26, 35–48.
- Tayfun, M., 1980. Narrow-band nonlinear sea waves. *J. Geophys. Res.* 85, 1548–1552.
- Tayfun, M., 1990. Distribution of large wave heights. *J. Waterway, Port, Coastal Ocean Eng.* 116, 686–707.
- Tayfun, M., Alkhalidi, M., 2020. Distribution of sea-surface elevations in intermediate and shallow water depths. *Coastal Eng.* 157.
- Tayfun, M.A., 1983. Frequency analysis of wave heights based on wave envelope. *J. Geophys. Res. Oceans* 88, 7573–7587.
- Tayfun, M.A., Fedele, F., 2007. Wave-height distributions and nonlinear effects. *Ocean Eng.* 34, 1631 – 1649.
- Tayfun, M.A., Lo, J.M., 1989. Envelope, phase, and narrow-band models of sea waves. *J. Waterway, Port, Coastal Ocean Eng.* 115, 594–613.
- Toffoli, A., Benoit, M., Onorato, M., Bitner-Gregersen, E., 2009. The effect of third-order nonlinearity on statistical properties of random directional waves in finite depth. *Nonlinear Processes in Geophysics* 16, 131–139.
- Toffoli, A., Bitner-Gregersen, E., Onorato, M., Babanin, A., 2008. Wave crest and trough distributions in a broad-banded directional wave field. *Ocean Engineering* 35, 1784–1792.
- Toffoli, A., Proment, D., Salman, H., Monbaliu, J., Frascoli, F., Dafilis, M., Stramignoni, E., Forza, R., Manfrin, M., Onorato, M., 2017. Wind generated rogue waves in an annular wave flume. *Physical Review Letters* 118.
- Trulsen, K., Dysthe, K.B., 1997. Freak waves – a three-dimensional wave simulation. in: Proc. 21st Symposium on Naval Hydrodynamics .
- Tung, C., Huang, N., 1985. Peak and trough distributions of nonlinear waves. *Ocean Eng.* 12, 201–209.
- Walker, D., Taylor, P., Taylor, R., 2004. The shape of large surface waves on the open sea and the draupner new year wave. *Appl. Ocean Res.* 26, 73–83.
- Waseda, T., Kinoshita, T., Tamura, H., 2009. Evolution of a random directional wave and freak wave occurrence. *Journal of Physical Oceanography* 39, 621–639.
- Winterstein, S., 1988. Nonlinear vibration models for extremes and fatigue. *J. Eng. Mech.* 114, 1772–1790.
- Winterstein, S., Ude, T., Marthinsen, T., 1994. Volterra models of ocean structures: Extreme and fatigue reliability. *J. Eng. Mech.* 120, 1369–1385.
- Zakharov, V., 1968. Stability of periodic waves of finite amplitude on the surface of a deep fluid. *Sov. Phys. J. Appl. Mech. Tech.* 9, 190–194.